MEMS magnetic field sensor based on silicon bridge structure*

Du Guangtao(杜广涛), Chen Xiangdong(陈向东)†, Lin Qibin(林其斌), Li Hui(李辉), and Guo Huihui(郭辉辉)

(School of Information Science and Technology, Southwest Jiaotong University, Chengdu 610031, China)

Abstract: A MEMS piezoresistive magnetic field sensor based on a silicon bridge structure has been simulated and tested. The sensor consists of a silicon sensitivity diaphragm embedded with a piezoresistive Wheatstone bridge, and a ferromagnetic magnet adhered to the sensitivity diaphragm. When the sensor is subjected to an external magnetic field, the magnetic force bends the silicon sensitivity diaphragm, producing stress and resistors change of the Wheatstone bridge and the output voltage of the sensor. Good agreement is observed between the theory and measurement behavior of the magnetic field sensor. Experimental results demonstrate that the maximum sensitivity and minimum resolution are 48 mV/T and 160 μT, respectively, making this device suitable for strong magnetic field measurement. Research results indicate that the sensor repeatability and dynamic response time are about 0.66% and 150 ms, respectively.

Key words: silicon bridge; magnetic field sensor; ferromagnetic magnet; ANSYS simulation; magnetic pressure; MEMS

DOI: 10.1088/1674-4926/31/10/104011 **EEACC:** 3100

1. Introduction

Flux gate magnetic field sensors[1, 2] and Hall-effect devices[2] are widely used to measure magnetic fields[3]. However, the operating power requirements of these devices are typically prohibitive for a long-term, portable application[3]. To meet the demands of miniaturization, lower requirement and low cost, a MEMS magnetic field sensor has been developed since the 1990s[4]. MEMS technology can be used to reduce the size of many types of sensors as well as increase their ability to be mass produced (e.g. pressure sensors and accelerometers).

Recently, the magnetic field sensors using MEMS technology have been reported in several studies[5–8]. Liu *et al.*[5] fabricated a cantilever magnetometer with a sensitivity of the order of 4.58 μT. Yang *et al.*[6] proposed a ferromagnetic magnetic field sensor that consists of low-stress electrodeposited magnetic alloys and surface-micromachined polysilicon structures and achieved a sensitivity of 200 nT. Behreyni *et al.*[7] reported a resonant MEMS magnetic field sensor with a minimum detectable signal of the order of 217 nT. Vasquez *et al.*[8] proposed a zero-power-magnetometer design which consists of a permanent magnet that is torsionally suspended to allow rotation about a single axis.

We proposed a novel method of fabricating a MEMS magnetic field sensor using a silicon bridge structure and incorporating a ferromagnetic magnet (FMM) as the sensing element. Improvement of the sensor sensitivity was achieved by selecting the materials and device geometry that would: (1) maximize the magnetic force resulting from the interaction between the external field and the ferromagnetic magnet, and (2) emphasize its effect on the sensor output. In this prototype device the mechanical response was measured and a sensitivity of 48 mV/T was achieved.

2. Principle

Figure 1 illustrates a schematic of the novel magnetic field sensor design. It consists of a silicon bridge structure and an FMM structure by the epoxy adhesive attaching to the sensitivity diaphragm. The silicon bridge has four piezoresistors placed along the periphery of the sensitivity diaphragm that are connected with a Wheatstone bridge configuration.

An FMM is characterized by the property of being "magnetized" if submitted to an external magnetic field. When the magnet is subjected to an external magnetic field, the relationship between the magnetic force and the magnetic field intensity B is[5]:

$$F = \frac{1}{2\mu_0} B^2 S, \tag{1}$$

where F is the magnetic force, μ_0 is the permeability of free space, and B and S are the magnetic field intensity and the area of FMM perpendicular to the magnetic field, respectively.

The interaction between an external magnetic field and the magnet generates a magnetic force which bends the silicon sensitivity diaphragm, producing stress and resistors change of the Wheatstone bridge and the output voltage of the sensor, as described in Fig. 2. The Wheatstone bridge output voltage U_0 is

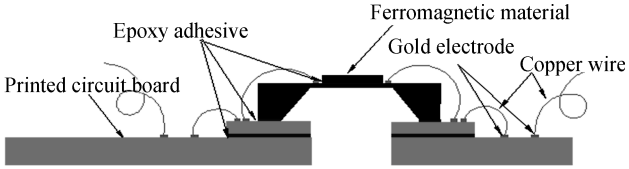

Fig. 1. Schematic of the proposed magnetic field sensor.

* Project supported by the National Natural Science Foundation of China (No. 60871024).

† Corresponding author. Email: xdchen@home.swjtu.edu.cn

Received 19 March 2010, revised manuscript received 20 May 2010

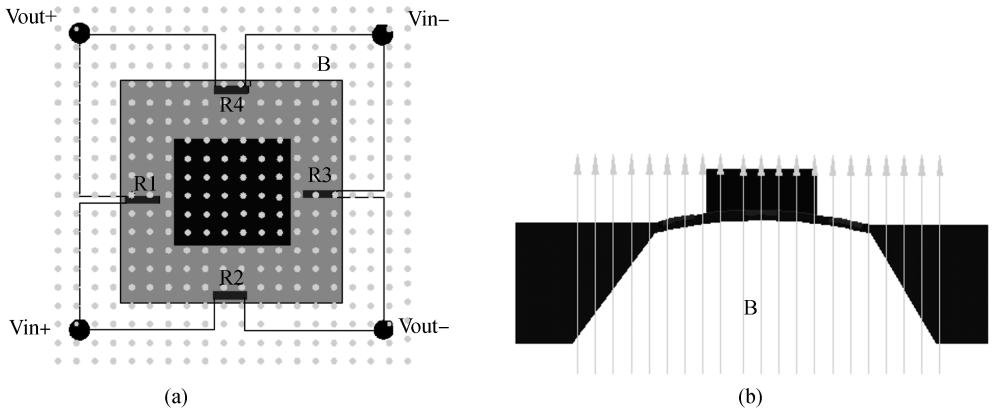

Fig. 2. Deformation of the magnetic field sensor with magnetic field. (a) Top-view. (b) Cross-section.

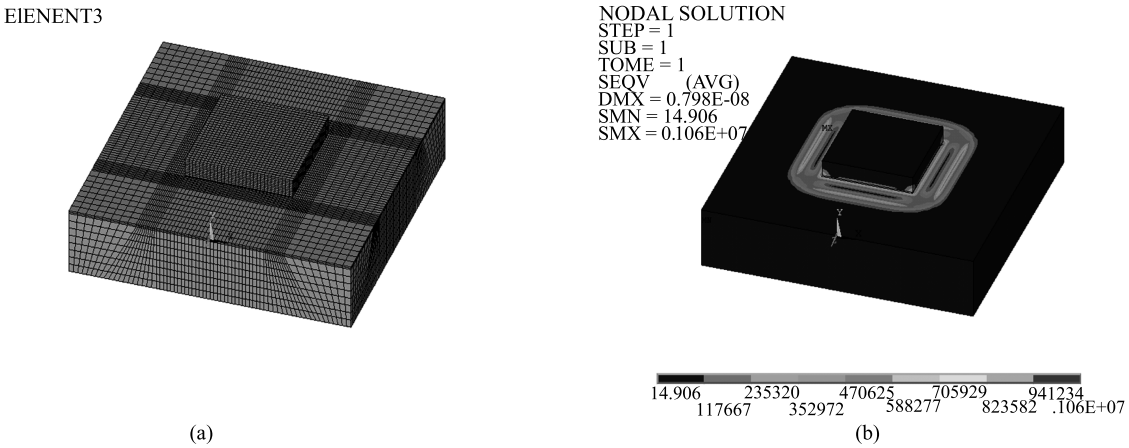

Fig. 3. 3D finite element model of the magnetic field sensor and the stress distributions. (a) Finite element model of magnetic field sensor. (b) The contour plot of membrane stress at the magnetic pressure of 5 kPa.

a linear function of the mechanical stress in the resistors perpendicular σ_{L} and parallel σ_{Q} to the diaphragm edge[9]:

$$U_0 = -\frac{\pi_{44}}{2} U_{\mathrm{I}}(\sigma_{\mathrm{L}} - \sigma_{\mathrm{Q}}) = -\frac{\pi_{44}}{2} U_{\mathrm{I}} \sigma_{\mathrm{Res}}, \tag{2}$$

where π_{44} denotes the piezoresistive coefficient of (100) ⟨110⟩-orientated silicon, and U_{I} is the operating voltage.

According to the small-deflection theory[10], the silicon sensitivity diaphragm displacement is small ($\omega_0 \leqslant 0.1h$, ω_0 is the deflection of the center of sensitive diaphragm) compared to the thickness of the silicon sensitivity diaphragm under transverse load pressure. The failure stress σ_{m} of silicon is 7×10^9 N/m^2[11]. The maximum stress $\sigma_{\max}$ of silicon in the status of small deflection should satisfy:

$$\sigma_{\max} \leqslant 0.2\sigma_{\mathrm{m}}. \tag{3}$$

Equation (3) could provide a reference for the calculation of maximum magnetic field measurement range.

3. Finite element simulation

Finite element modeling and simulation were performed using the software package ANSYS. All mechanical parameters are listed in Table 1. The response of the magnetic field sensor is represented by a constant magnetic pressure (magnetic pressure is defined as the ratio between the magnetic force of FMMs to the upper bases area of the magnet) applied to the upper bases of the FMM.

Table 1. Parameters for ANSYS simulation.

Material	Elastic modulus (GPa)	Poisson ratio	Density (g/cm^3)
Silicon	150	0.23	2.23
Epoxy adhesive	3.5	0.38	1.96
Bearing steel	208	0.3	7.85

The magnetic field sensor model used for simulation is shown in Fig. 3(a). The SOLID45 element is used to model the silicon bridge and FMM. The MEMS200 element is used for the epoxy adhesive. The regular prism bearing steel FMMs is 120 μm high. We simulated devices with different side lengths of FMM to investigate their effect on the magnetic field sensor performance. Figure 4 illustrates the performance of magnetic field sensors with different side lengths and the same altitude. From Fig. 4, it is observed that the side length should be around 0.7 mm for maximum sensitivity. So we only focus on the FMM with a side length of 0.7 mm for discussion. Fig-

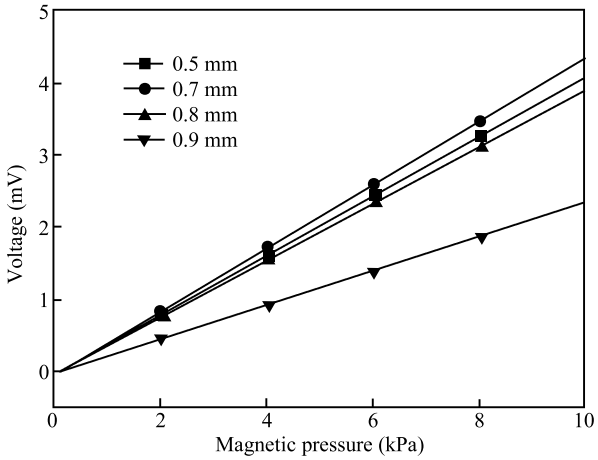

Fig. 4. Response curves between magnetic pressure and magnetic field intensity with different side lengths.

ure 3(b) is the contour plot of sensitive membrane stress distribution with magnetic pressure of 5 kPa perpendicular to the upper bases of the magnet which has the dimensions of 700 × 700 × 120 μm^3. It is observed that the maximum stress occurs at the middle edge of the square diaphragm. The piezoresistors are placed at the edges of the square diaphragm to gain maximum sensitivity. By changing the magnet surface magnetic pressure, we obtained the midpoint stress value of the sensitive diaphragm edge, and the sensor output voltage is determined by Eq. (2). Further, the relationship between magnetic pressure and output is gained, as shown in Fig. 5(a).

Figure 5(b) shows the theory curves obtained by Eq. (1) between the magnetic pressure on the magnets upper surface and the magnetic field intensity. Equation (1) has no consideration of the magnetic force of the magnet side. Actually, the magnetic force of the magnet side is less than the magnet upper surface magnetic force. As can be seen from Figs. 5(a) and 5(b), the theory curve between the magnetic field intensity and the sensor output voltage can be obtained in Fig. 5(c).

4. Fabrication

In this paper, the sensor with the FMM side length of 0.7 mm is prepared for test. The silicon bridge fabrication process is mature, which is described in Ref. [12]. In Ref. [12], the starting material used is silicon with (100) oriented and n-type doped. The fabrication process flow is as follows.

(1) Thermal silicon oxide growth and LPCVD polysilicon deposition on the silicon oxide.

(2) Photolithographic steps and boron ion implantation for four polysilicon piezoresistor.

(3) A metal Al layer is deposited via sputtering. The second photolithographic steps are used to make Al electrodes and form the Wheatstone bridge configuration.

(4) The second metal Al layer is deposited on the backside silicon via sputtering.

(5) The third photolithography step and etching Al layer. Then the alloy step is performed.

(6) Etching of the backside silicon. The silicon diaphragm thickness is 75 μm.

(7) Backside Al layer removal by wet etching.

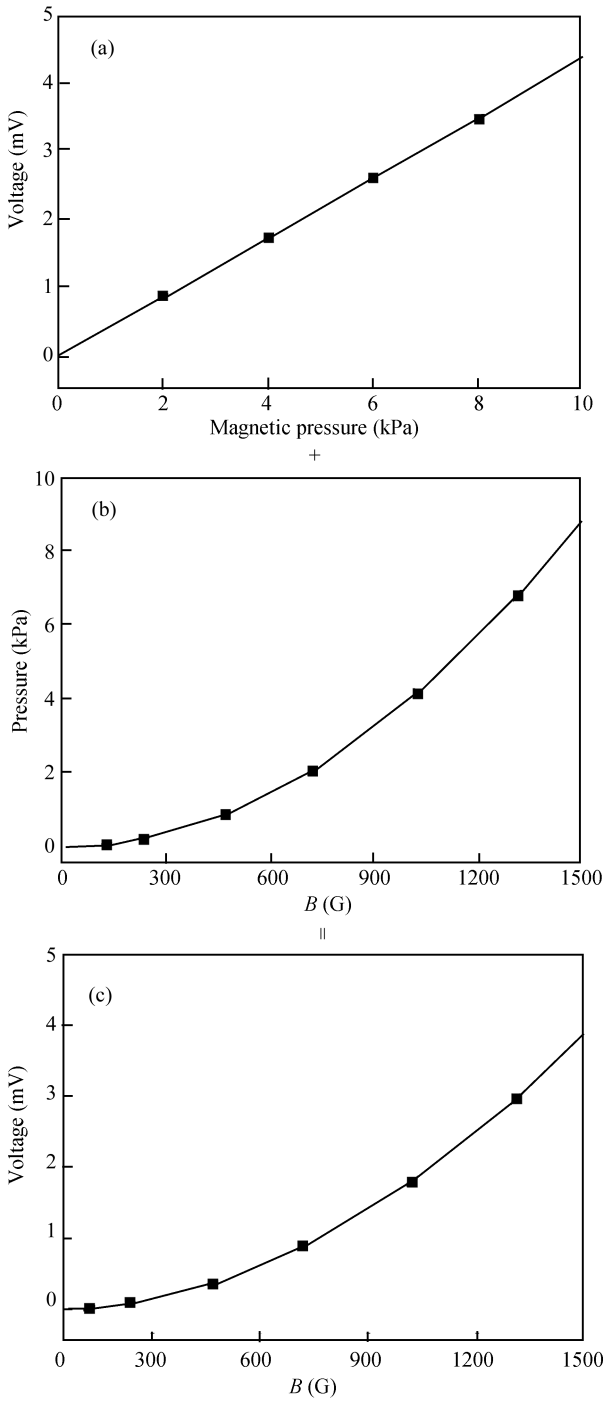

Fig. 5. (a) Theory relationship between the magnetic pressure and the output with a side length of 0.7 mm. (b) Theory curve between the magnetic field intensity and the magnetic pressure. (c) Theory curve between the magnetic field intensity and the output voltage.

In Fig. 6 a photograph of the pressure sensor chip in Ref. [12] is shown. The MEMS pressure sensor has measured sensitivity of 0.151 mV/kPa when the power supply is 5 V.

In this paper, the silicon bridge sensitivity diaphragm has dimensions of about 1100 × 1100 × 20 μm^3. The fabricated silicon bridge has a sensitivity 8.9 times that of the pressure sensor in Ref. [12] when working at 5 V. The starting material used is silicon with (100) oriented and n-type doped. The fabrication process flow is as follows.

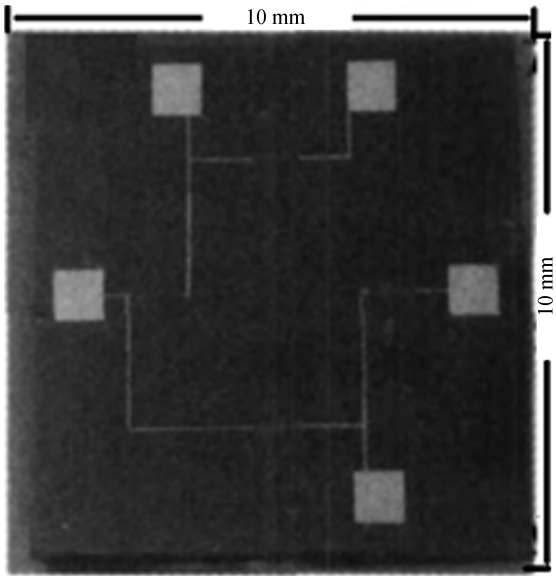

Fig. 6. Photograph of the pressure sensor chip in Ref. [12].

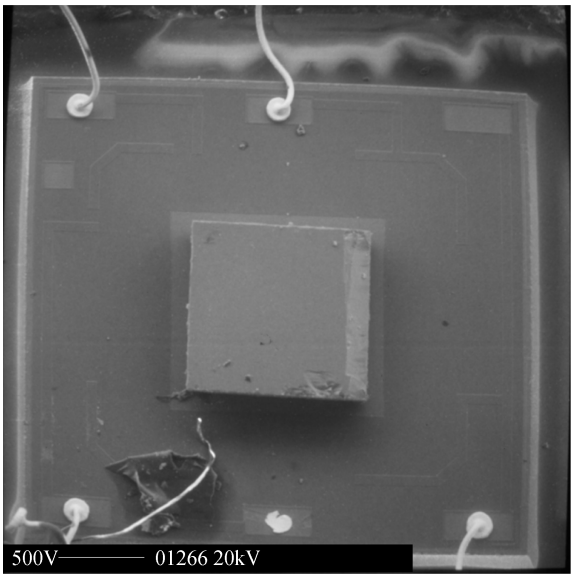

Fig. 7. SEM photograph of the magnetic field sensor.

(1) Thermal silicon oxide growth.

(2) Photolithographic steps and boron ion implantation for four piezoresistor.

(3) A metal Al layer is deposited via sputtering. The second photolithographic steps are used to make Al electrodes and form the Wheatstone bridge configuration.

(4) The second metal Al layer is deposited on the backside silicon via sputtering.

(5) The third photolithography step and etching Al layer. Then the alloy step is performed.

(6) Etching of the backside silicon. The silicon diaphragm thickness is 20 μm.

(7) Backside Al layer removal by wet etching.

After the completion of the silicon bridge, it was glued to a PCB with gold electrodes as electrical connection for fixation. In the center of the PCB, it has a blowhole which can make the silicon bridge have the same atmospheric pressure inside and outside the cavity to avoid temperature influence. The FMM (height = 120 μm and side length = 0.7 mm) was then glued on the center of the sensitive membrane under a microscope. The SEM photograph of the fabricated magnetic field sensor is shown in Fig. 7.

5. Experiment and results

The performance of the prepared sensor was tested at atmospheric pressure and room temperature. The sensor was placed in the middle of the two magnetic poles of the electromagnet that generated a homogeneous magnetic field perpendicular to the upper and lower bases of the FMM. Variation of the magnetic field intensity was achieved by controlling the current flowing through the coil. A supply voltage of 5 V was applied to the magnetic field sensor. The set-up is pictured in Fig. 8.

For magnetic sensing assessment, a homogeneous magnetic field was varied from 0 to 1500 G by controlling the current source. Figure 9 illustrates the voltage output of the magnetic field sensor as a function of external magnetic field intensity. To compare the results of theory and measurement, Figure 10 additionally contains the theory curve.

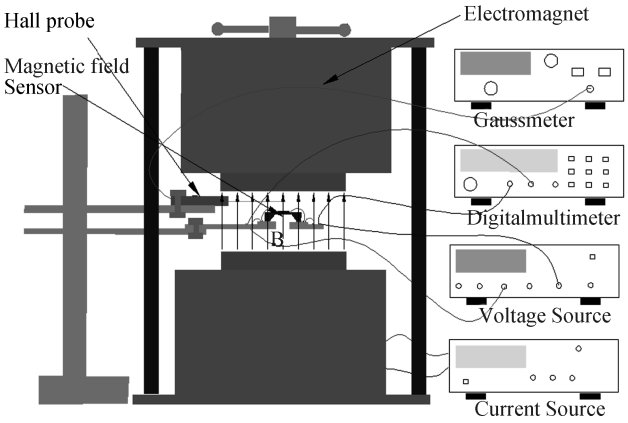

Fig. 8. Complete test set-up of the magnetic field sensor.

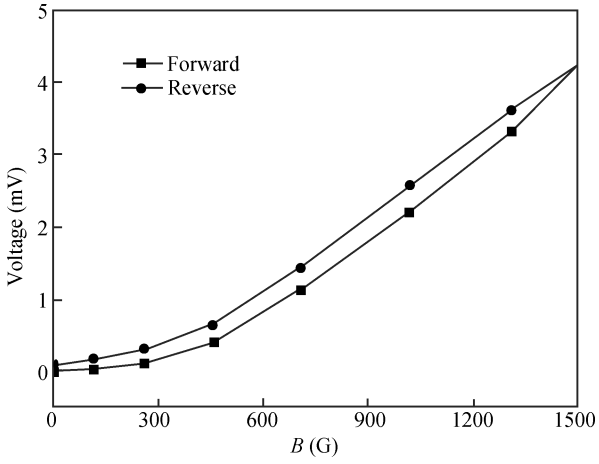

Fig. 9. Response characteristics of the magnetic field sensor.

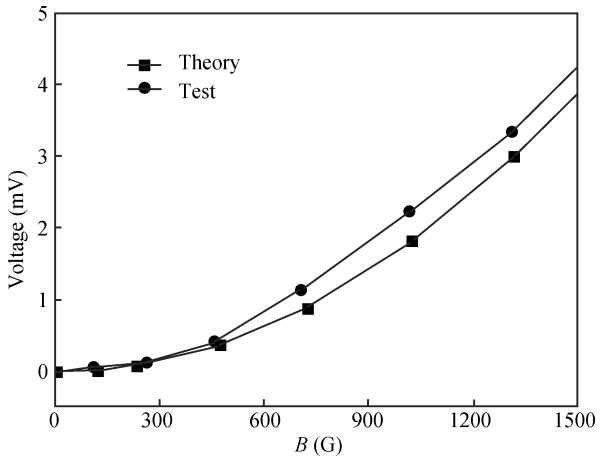

Fig. 10. Comparison of theory and test.

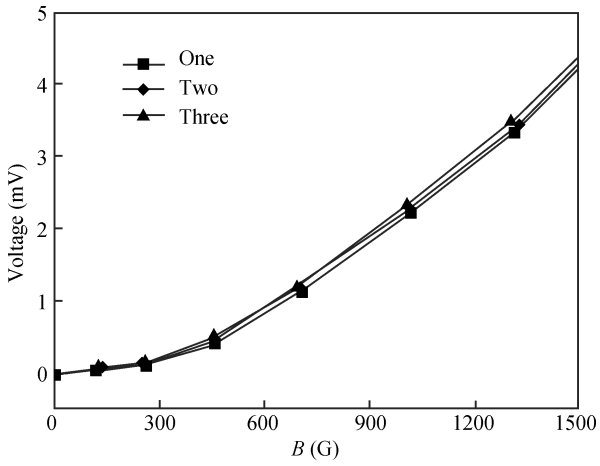

Fig. 11. Repeatability characteristic.

5.1. Repeatability

By testing three times, we obtained the repeatability curve in Fig. 11. The experimental results demonstrate that the repeatability is good. In order to measure the repeatability characteristic, the ratio of maximum output deviation $\Delta_{\max}$ to full-scale y_{FS} is defined:

$$\delta_{\mathrm{R}} = \pm\frac{\Delta_{\max}}{y_{\mathrm{FS}}} \times 100\% = \pm 0.66\%. \tag{4}$$

5.2. Dynamic performance analysis

To verify the dynamic performance of the sensor, the magnetic field intensity was adjusted to 1500 G firstly. Then the power supply of the electromagnet was turned off. Agilent34401A was connected to a computer to acquire the output voltage of the sensor automatically. Thirdly, we turned on the multimeter and electromagnet power supply. After the multimeter had acquired data for a short time, the electromagnet power supply was turned off again. Finally, the sensor dynamic response curve was obtained (Fig. 10). Figure 12 indicates that the response time of the sensor was about 150 ms.

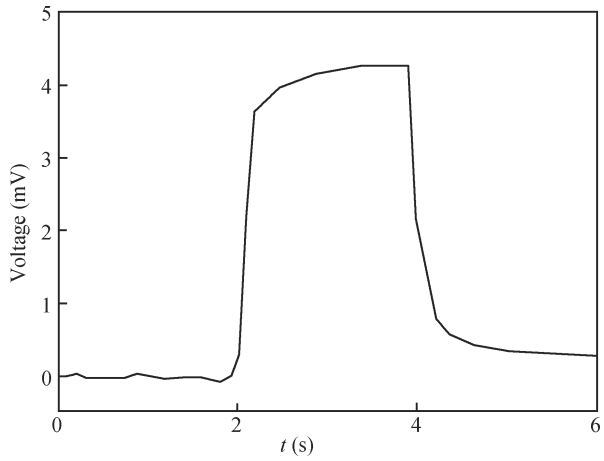

Fig. 12. Dynamic performance.

6. Discussion

The experimental result shown in Fig. 10 is close to the theoretical values. Due to omitting the magnet side magnetic force, the theory result is less than the measurement result. In addition, when the FMM was subject to a homogeneous magnetic field generated by the electromagnet, there will be edge effects which lead to different magnetic field intensity on the upper and lower surfaces of FMM, so this may cause a deviation between the theory and the test. Furthermore, the deviation recorded in Fig. 10 also comes from the positioning error of the testing location in the magnetic field. Both the probe of the Gaussmeter and the magnetic field sensor cannot be placed very precisely in the experiment. In Fig. 10, it was observed that the maximum sensitivity and minimum resolution were 48 mV/T and 160 μT, which is better than the "U-shape" cantilever[13] with 14 mV/T in sensitivity and 380 μT in resolution.

These three repeatability curves (Fig. 11) almost coincide with each other because of the same test conditions. The small deviation is due to the remanence of the electromagnet and FMM.

The dynamic performance curve (Fig. 12) must be a deviation because of the time spent turning the electromagnet and multimeter power supply on and off. The actual response time should be less than 150 ms.

The silicon bridge used for the magnetic field sensor in this paper has the maximal output voltage of 160 mV. In this case, the stress difference is 4.6×10^7 Pa by Eq. (2), which is much smaller than $\sigma_{\max}$ of Eq. (2). In accordance with Fig. 5(a), it was shown that a magnetic pressure of 366.3 kPa can lead to a 4.6×10^7 Pa stress difference. A magnetic field intensity of 9593 G produces a magnetic pressure of 366.3 kPa by Fig. 5(b). The actual measurement range of the proposed magnetic field sensor is 1.6–9593 G if the magnetic field intensity is no more than the saturation magnetic flux density of bearing steel. The measurement range of silicon Hall magnetic field sensors is 10–1000 G, which is less than the proposed sensor. The estimated power consumption of the device is then 5 mW, which is less than silicon Hall magnetic field sensor power[2].

Figure 7 indicates that the magnetization of FMM has a hysteresis dependence on the magnetic field. To reduce the hys-

teresis, we can take into account the low coercivity materials (e.g. NiFe alloy[14]).

7. Conclusions

We have proposed a structure of a MEMS ferromagnetic magnetic field sensor based on a silicon bridge. The device has been successfully used for strong magnetic field measurement. Operated at a low voltage (5 V), the fabricated sensor has a maximum sensitivity of 48 mV/T and a measurement range of 1.6G–9593G if the magnetic field intensity is no more than the saturation magnetic flux density of bearing steel. The repeatability and dynamic response time are about 0.66% and 150 ms, respectively. The theoretical results agreed well with the experimental results. The proposed magnetic field sensors have mature fabrication technology, cost-effective batch fabrication, low cost, lower power, small area and easy integration. More work can be done to improve the sensor performance by selecting the FMM materials and geometry.

Acknowledgements

The authors thank Xiao H. B. for simulation discussions.

References

[1] Yang Jianzhong, You Zheng, Liu Gang, et al. Micro fluxgate magnetometer named MEMSMag. Journal of Functional Materials and Devices, 2008, 14(2): 313 (in Chinese)

[2] Lenz J, Edelstein A S. Magnetic sensors and their application. IEEE Sensors J, 2006, 6(3): 631

[3] Seungkeun C, Seong-Hyok K, Yong-Kyu Y, et al. A magnetically excited and sensed MEMS-based resonant compass. IEEE Trans Magn, 2006, 42(10): 3506

[4] EDonizier E, Lefort O, Spirkovitch S, et al. Integrated magnetic field sensor. Sensors and Actuators, 1991, 25–27: 357

[5] Liu J, Li X X. A piezoresistive microcantilever magnetic-field sensor with on-chip self-calibration function integrated. Microelectron J, 2007, 38(2): 210

[6] Yang H H, Myung N V, Yee J, et al. Ferromagnetic micromechanical magnetometer. Sensors and Actuators A, 2002, 97/98: 88

[7] Behreyni B, Shafai C. A resonant micromachined magnetic field sensor. IEEE Sensors J, 2007, 7(9): 1326

[8] Vasquez D J, Judy J W. Optically-interrogated zero-power MEMS magnetometer. J Microelectromech Syst, 2007, 16(2): 336

[9] Buchhold R, Nakladal A, Gerlach G, et al. Design studies on piezoresistive humidity sensors. Sensors and Actuators B, 1998, 53(1/2): 1

[10] Zhao L L, Xu C, Shen G D. Analysis for load limitation of square-shaped silicon diaphragms. Solid-State Electron, 2006, 50(9/10): 1579

[11] Pertersen K E. Silicon as a mechanical material. Proc IEEE, 1982, 70: 420

[12] Zhao Xiaofeng, Wen Dianzhong. Fabrication and characteristics of a nano-polysilicon thin film pressure sensor. Journal of Semiconductors, 2008, 29(10): 2038 (in Chinese)

[13] Beroulle V, Bertrand Y, Latorre L, et al. Monolithic piezoresistive CMOS magnetic field sensors. Sensors and Actuators A, 2003,103(1/2): 23

[14] Niarchos D. Magnetic MEMS: key issues and some applications. Sensors and Actuators A, 2003, 109(1/2): 166